Year-round observations of carbon biomass and flux variability in the Southern Ocean

James K. B. Bishop[1,2] and Todd J. Wood[2]

Received 26 February 2008; revised 17 February 2009; accepted 17 March 2009; published 16 June 2009.

[1] Three Carbon Explorer (CE) floats profiling to kilometer depths in the Southern Ocean tracked dawn-dusk variations of mixing and stratification, particulate organic carbon, and light scattering and sedimentation at 100, 250, and 800 m continuously from January 2002 to April 2003. Data were analyzed in conjunction with contemporaneous satellite winds and chlorophyll and derived subsurface light fields. The CE deployed at 66°S, 172°W operated in the ice edge zone in absence of light. Two CEs deployed at 55°S, 172°W recorded wintertime mixing to ~400 m yet observed very different bloom dynamics and sedimentation the following spring. Four hypotheses are explored. The strongest hypothesis is that shallow transient stratification of the deep winter mixed layer to shallower than photosynthetic critical depth occurred more frequently in the nonbloom, higher-sedimentation case. The lower particle export to 800 m under the bloom was hypothesized to be due to higher interception of sinking carbon by a relatively starved overwintering zooplankton population. In the Southern Ocean, surface phytoplankton biomass may counterindicate particle flux at kilometer depths.

Citation: Bishop, J. K. B., and T. J. Wood (2009), Year-round observations of carbon biomass and flux variability in the Southern Ocean, *Global Biogeochem. Cycles*, *23*, GB2019, doi:10.1029/2008GB003206.

1. Introduction

[2] Marine phytoplankton biomass turns over on average once every 1–2 weeks, yet these short-lived marine phytoplankton, which fix carbon at a rate of 40–50 pg C a^{-1}, account for roughly half of the global primary productivity [*Antoine et al.*, 1996; *Field et al.*, 1998; *Falkowski et al.*, 1998]. Approximately 10 pg C a^{-1} are exported below 100 m to the deep sea [*Volk and Hoffert*, 1985], mostly carried by sinking particles. This very fast process, commonly referred to as the ocean's "biological carbon pump," is important to the regulation of atmospheric CO_2. The fact that the strength of the biological carbon pump has been estimated through a grand averaging and inversion of global nutrient fields from ship observations collected over the past 6 decades means that it is not presently possible to know if the biological carbon pump is in steady state or not.

[3] The effectiveness of the biological pump may be negatively impacted by the now readily detected ocean uptake of the CO_2 added to the atmosphere by humans since the Industrial Revolution. The pH of today's surface ocean waters has decreased by ~0.1 unit since the Industrial Revolution [*Sabine et al.*, 2004; *Feely et al.*, 2004]. Models predict that continued ocean acidification will lead to a decline in the productivity of calcium carbonate forming coral reef communities, zooplankton (foraminifera and pteropods), and phytoplankton (coccolithophores) in the coming decades [*Orr et al.*, 2005]. Furthermore, because carbonate particles incorporated into fecal material are important contributors to excess density, that is, they are the "ballast" that causes these particles to sink [*Armstrong et al.*, 2001], a decrease of carbonate ballast would lead to slower aggregate sinking speeds, and thus, more organic matter remineralization will occur closer to the ocean surface, where waters are in more rapid exchange with the atmosphere. Changes to the pump brought about by global warming induced changes in ocean circulation and other human activities such as fisheries are simply not yet predictable.

[4] The only way to predict future trajectories of the global carbon cycle is through model simulations that accurately represent the substantial biotic carbon flows in the ocean; however, the parameterizations embedded within models for biotic carbon cycle processes represent the sum of knowledge derived from observations. Many of these observations are sparse in terms of time and space. For example, *Lam and Bishop* [2007] showed that carbon remineralization length scales are different during summer conditions north and south of the Antarctic Polar Front (APF); *Buesseler et al.* [2007] found very different remineralization length scales during summertime conditions in oligotrophic waters near Hawaii versus productive waters of the Oyashio Current near Japan. Many ocean biogeochemistry models still use a single space- and time-invariant remineralization length scale derived from *Martin et al.*'s [1987] fair weather observations in the Pacific and cannot

[1]Department of Earth and Planetary Science, University of California, Berkeley, California, USA.
[2]Earth Sciences Division, Lawrence Berkeley National Laboratory, Berkeley, California, USA.

0886-6236/09/2008GB003206$12.00

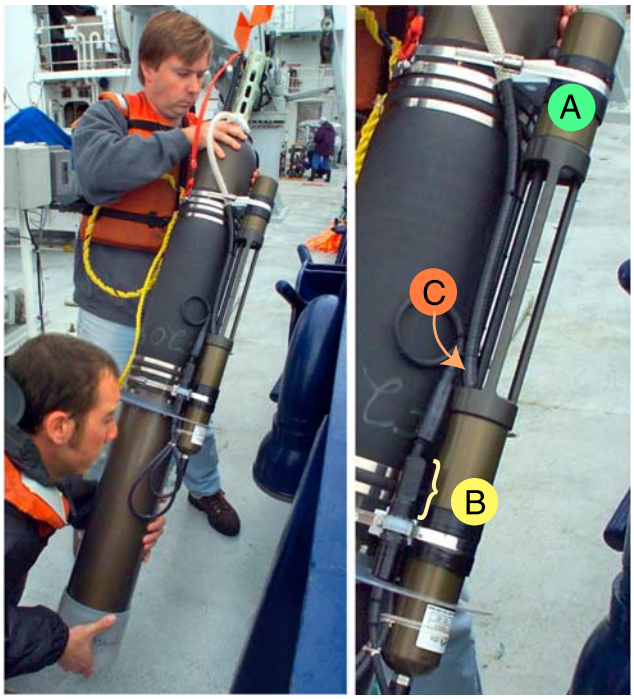

Figure 1. Carbon Explorer showing optical transmissometer (A) and scattering sensors (B). The transmissometer has been configured to permit the determination of the systematic variations of carbon sedimentation. While the float is at depth between profiles, particles accumulate on the upward looking window (C) of the transmissometer. Prior to profile operations, the transmissometer is read, the window is flushed clean with flowing seawater, and the transmission reading is determined a second time. The difference in transmission normalized by time at depth between profiles is the carbon flux index (CFI).

capture the impact of changes in ballast, among other things, on the global carbon cycle.

[5] Autonomous technology promises to overcome the space-time gap in ocean carbon observations. The international program Argo [*Argo Science Team*, 1999] has seeded the world's oceans with 3000 low-cost autonomous profiling floats to gather widespread temperature and salinity profiles and information on middepth circulation for investigation of the climate state of the ocean. Argo floats are designed to profile to the surface from kilometer depths once every 10 days and record deep currents between profiles over 5 years.

[6] The Carbon Explorer (CE), which is described in section 2, is a telemetry- and optical sensor–enhanced Argo float designed and programmed to capture the fast diurnal physical and biological linkages and processes of the ocean's biological carbon pump [*Bishop et al.*, 2002]. Here we report on yearlong continuous CE deployments in the Southern Ocean, an area of sparse carbon observations, yet critically important to the carbon cycle. Two CEs were deployed at 55°S, 172°W, north of the Antarctic Polar Front (APF) in the Southern Ocean during the January–February 2002 Southern Ocean Iron Experiment (SOFeX) [*Coale et al.*, 2004] (one as control and the other in iron-amended waters; we refer to these as CE 55C and CE 55A, respectively). A third CE (CE 66A) was deployed (also during SOFeX) at 66°S, 172°W, south of the APF. A strong (but unexpected in low-silicate, high-nitrate subantarctic waters), iron-stimulated plankton bloom and subsequent enhanced sedimentation through 100 m [*Bishop et al.*, 2004] was observed over 60 days at 55°S.

[7] The three CEs continued profiling in the Southern Ocean for another 14 months after the effects of SOFeX iron were no longer detectable. The 66°S CE observed particulate organic carbon (POC) dynamics in the seasonal ice influenced waters, survived one Antarctic winter, and continued for a total of 18 months into the next winter season. Ship-based observations would have been impossible because of the prohibitive cost and extreme environmental conditions. This paper reports, for the first time, year-round high-frequency observations of surface biomass and carbon export to depth in the Southern Ocean. A central question investigated is how and if surface biomass fields detected by satellite remote sensing may be used to predict carbon sedimentation to depth and, if not, what biogeochemical mechanisms are in action.

2. Methods

[8] The Carbon Explorer (CE) (Figure 1), like all Argo floats, can autonomously collect hundreds of profiles of temperature (T), salinity (S), and pressure (Sea-Bird Electronics, Inc., Seattle, Washington) to kilometer depths and communicate data to shore via satellite in near real time. Unlike Argo floats, the CE is outfitted with a neutrally buoyant transmissometer (WETLabs Inc., Philomath, Oregon) to measure particulate organic carbon (POC) concentration while profiling and carbon flux index (CFI) while drifting at depth between profiles (Figure 2). CFI is the transmittance signal anomaly due to the accumulation of particles on the upward looking transmissometer window normalized by the time the float is at depth; specifics are described in detail by *Bishop et al.* [2004]. An added light scattering sensor (0.03 W power, Seapoint Sensors, Inc., Exeter, New Hampshire) was used to cross-check the transmissometer. Each CE uses fast bidirectional satellite (ORBCOMM) telemetry, which permits efficient uplink of data in minutes and postdeployment changes to mission parameters such as profiling depths, drift depths, and profiling frequency.

[9] Three CEs (floats 1177, 2054, and 2104) were deployed in January 2002 during the Southern Ocean Iron Experiment (SOFeX) near 55°S, 172°W. One CE (float 2103) was deployed in iron-amended waters near 66°S, 172°W.

[10] A fourth explorer, CE 2054, was deployed in iron-amended waters but failed early in its mission. CE 2104 was deployed 10 days later, again in iron-amended waters. The early record for CE 2054 was combined with the complete record of CE 2104, and in this paper we describe this record as CE 55A (the "55" denotes deployment latitude (°S), and the "A" denotes "iron-amended"). The record from CE 1177, deployed as a control in untreated waters, is

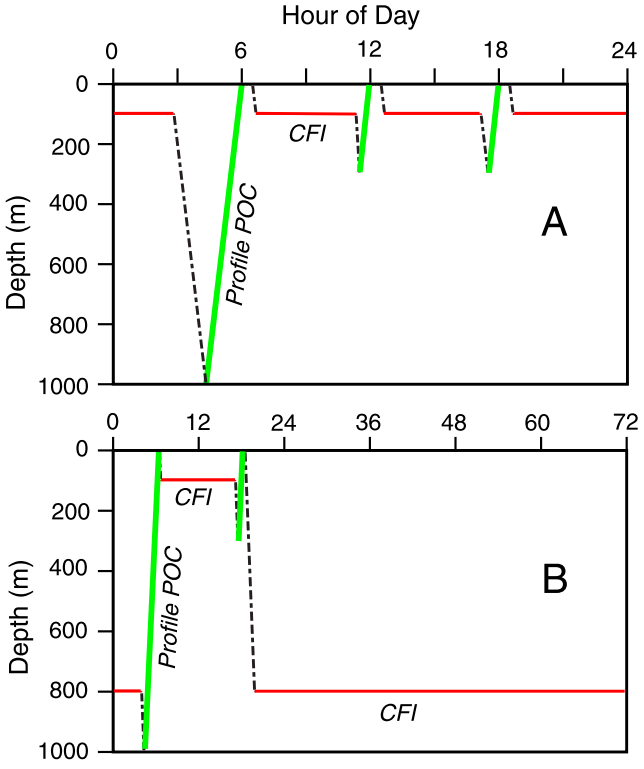

Figure 2. Carbon Explorer mission profiles (a) during the 2002 Southern Ocean Iron Experiment (SOFeX) and (b) post-SOFeX. Green solid lines indicate times of profiling (T, S, scattering, transmission). Red solid lines indicate periods of determination of carbon flux index (CFI) while the float is parked and inactive at depth. At each surfacing, the CE obtains a GPS position, listens for commands, and sends data to satellite. CEs deployed during SOFeX profiled 300,000–400,000 m over their lifetimes.

referred to as CE 55C ("C" for "control"). Similarly, the record for CE 2103 will be referred to as CE 66A.

[11] Both CE 55A and CE 55C measured CFI at 100 m depth (when not profiling) and profiled upward from 1000, 300, and 300 m on a dawn, midday, and dusk schedule (0600, 1200, and 1800 local solar time (LST)). On day 70 (day 1 is 1 January 2002), CE 55C was reprogrammed to skip the midday profile and to measure CFI alternately at 100 and 800 m; on day 120, CFI depth was changed from 100 m to 250 m. On day 80, CE 55A was reprogrammed to skip its midday profile and to alternate between CFI depths of 100 and 800 m. During the wintertime, the duration of the 800 m CFI measurement for both floats was extended to several days as a power-conserving strategy. CE 66A initially was programmed to profile daily from 1000 m to surface at "dawn" (0600 LST) and to measure CFI at 100 m. Its profiling frequency was decreased to once per week as it began to encounter sea ice. Once the ice began to retreat, the frequency was increased to once every 3 days.

[12] Transmissometer data were processed to particle beam attenuation coefficient (c_p in m^{-1}) and then POC (in μM) as described by *Bishop et al.* [2004]. Steps included (1) verification of initial CE transmissometer calibration (postdeployment) with a ship-deployed transmissometer, (2) compensation for biofouling using a fixed optical reference in the nearly particle free water at 1000 m, (3) multiplication of c_p by a factor of 1.3 to compensate for the specifics of the beam and detector geometry of the transmissometer used [see also *Bishop and Wood*, 2008], (4) correction for small pressure-proportional offset of c_p (0.003 m^{-1} over 1000 m) for data from one CE (float 2104), and (5) multiplication of scaled c_p by factors of 16.1 μM C m^{-1} for CEs 55A and 55C and 27.4 μM C m^{-1} for CE 66A.

[13] CEs 55A and 55C were operating near the service edge of ORBCOMM, the communication satellite system (~55°S), but achieved better than 90% transmission efficiency. GPS positions, profile data, and CFI data were transmitted each time the CE surfaced in a matter of minutes (weather permitting; weather not permitting, the data were retained for later transmission using a last in–first out protocol up to a limit of ten profiles of information). CE 66A lost much more data because of marginal satellite service. Remarkably, CE 66A's data transmission greatly improved during the winter because of the combined effects of wave damping by surrounding sea ice and the high viscosity of near-freezing surface seawater.

[14] The records of the CEs in Antarctic waters are significant since they were operating in the extreme conditions of the Southern Ocean, where average wind speeds are >10 m s^{-1} year-round. To provide some context, only 5 of 1600 project Argo floats were operating south of 60°S in January 2005, 3 years after our deployments.

3. Results

[15] CEs 55A and 66A were both deployed in iron-amended waters and registered the initial biomass enhancement near the surface. The signal of the iron-stimulated plankton growth and sedimentation ended after 2 months at 55°S and after 2 weeks at 66°S [*Bishop et al.*, 2004]. The control CE 55C saw none of the SOFeX iron. The CEs went on to observe the natural physical and biological processes of the Southern Ocean from February 2002 through April 2003 (CE 66A much longer). After 400 days, CEs 55C and 55A had tracked 3500 and 2200 km to the east, respectively (Figure 3), and each had transited a round-trip vertical profiling distance of ~400,000 m.

3.1. Lagrangian Drift and Seasonal Hydrographic Change

[16] The trajectories of the CEs revealed the major influence of seafloor topography on circulation, although the ocean bottom was 2 km or more below the deepest drift depth. CE 55C followed a meandering path eastward until it encountered and tracked parallel to the Udintsev Fracture Zone from days 195 to 215. It then turned to follow the crest of the Pacific-Antarctic Ridge to the northeast and on day 270 turned to track southeast above the Tharp Fracture Zone. CE 55A encountered and turned to track the Udintsev Fracture Zone 1 year after it was deployed. CE 66A followed the crest of the Pacific-Antarctic Ridge to the northeast, whereupon it too encountered and began a transit

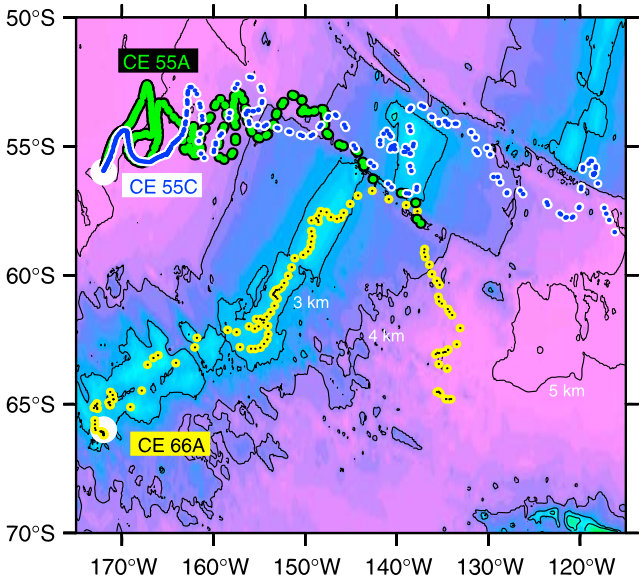

Figure 3. Bathymetric map showing tracks of Carbon Explorers deployed in January 2002 for SOFeX and indicating the importance of mid-ocean ridge and fracture zones in determining trajectories.

through the Udintsev Fracture Zone (on day 370, 5 January 2003). Such topographic effects have been reported for surface drifters deployed in the Polar Front Zone [*Abbott et al.*, 2001]; our observations confirm the observation of fracture zone preference for ridge-crossing floats deployed in the North Atlantic [*Bower et al.*, 2002; *Bower and von Appen*, 2008] and also reproduce the patterns of the large-scale intermediate circulation of the ocean [*Davis*, 2005].

[17] Although CE 55A and CE 66A passed above the same fracture zone in early January 2003 with tracks separated by ~50 km, they recorded distinctly different temperature and salinity signatures of their water masses (Figure 4). CE 66A recorded the classic thermal signature of winter water colder than −1°C at 100 m, while CE 55A recorded 5°C at the same depth.

3.1.1. Current Shear

[18] Analysis of the progressive drift displacements of CEs 55C and 55A once they were alternating their CFI depths between 100 or 250 m and 800 m (from March 2002 onward) revealed <50% difference in current strength between 100 and 800 m, consistent with the largely barotropic nature of the Circumpolar Current north of the APF. For example, during days 350–400 (a period of POC increase in surface waters and sedimentation described in section 4.2), CE 55A was advected 20 km d^{-1} (100 m) and 12 km d^{-1} (800 m); similarly, CE 55C was advected 14.5 km d^{-1} (250 m) and 10.3 km d^{-1} (800 m). Analysis of the explorer trajectories indicates that there was little course deviation between shallow and deep explorer positions (Figure 3). The current shear in the along-track direction was thus ~8 (CE 55A) and ~4 km d^{-1} (CE 55C). The displacement between the euphotic layer and 100 m was minimal since CE 55A followed the center of a small-scale patch of iron-amended water during the first 2 months of its mission despite being advected hundreds of kilometers from its deployment point and despite its yo-yoing to 1000 m and to 300 m (twice) each day.

3.1.2. Mixed Layer History

[19] The stratification and mixing behavior of the upper water column is a critical factor governing the subsurface light fields experienced by phytoplankton. The mixed layer depths (MLD) at which potential density increases from the surface value by 0.01‰ ($\Delta\sigma_\Theta$ = 0.01) and by 0.05‰ are measures of hourly and 24 h mixing, respectively [*Bishop et al.*, 2002, 2004]. In high-nutrient, low-chlorophyll waters, $MLD_{0.05}$ is often the depth below which POC concentrations strongly decline. This is true of the data presented here. $MLD_{0.01}$ is often the depth above which one can clearly see the effect of daytime POC growth in dusk profiles. The norm for seasonal mixing is ($\Delta\sigma_\Theta$ = 0.125). We denote mixing depths determined for hourly, daily, and seasonal time scales as MLD_{01}, MLD_{05}, and MLD_{125}, respectively.

[20] The time series of MLD_{05} for the three CEs revealed strong differences in the depth of wintertime mixing north and south of the APF (Figure 4). The greatest mixed layer depths occurred from day 210 to 300 (August to October 2002), and during this time, seasonal mixing (MLD_{125}) extended to 435 m (CE 55A) and 374 m (CE 55C) north of the APF and to 109 m (CE 66A) south of the APF. These observations are in agreement with *Morrison et al.* [2001]. On 24 h time scales (MLD_{05}), winter mixing extended to 335 m (CE 55A), 275 m (CE 55C), and 85 m (CE 66A).

[21] While the MLD_{05} averages for the two 55°S CEs during the deep mixing period were 20% different, the frequency-depth distribution of hourly mixing (MLD_{01}) when classified by time of day (0600 and 1800 LST; designated AM and PM, respectively) revealed major differences in the frequency occurrence of transient shallow stratification events (Figure 5). In the AM CE 55A data, MLD_{01} never occurred shallower than 150 m, but it occurred 30% of the time in the PM data set. In contrast, CE 55C AM data showed MLD_{01} shallower than 150 m 20% of the time and shallower than 100 m 30% of the time in the PM set. Many of the shallow MLD_{01} occurrences seen by CE 55C were clustered between days 270 and 300. As will be shown below, the phytoplankton populations in the mixed layers tracked by CE 55C consistently achieved net positive photosynthesis 30 days earlier than those observed by CE 55A prior to permanent stratification.

[22] Surface forcing differences explaining the MLD_{05} and MLD_{01} trends recorded by the CEs north of the APF are difficult to discern. For the period between days 210 and 300 (August to October 2002), averages of wind stress values calculated using NASA Quick Scatterometer (QuikSCAT) data, interpolated to the positions of CEs 55C and 55A, were 0.259 and 0.252 Pa, respectively. The standard deviation of wind stress was similarly almost identical (0.180 and 0.175 Pa, respectively). Surface solar irradiance calculated using clear-sky irradiance climatology of *Bishop et al.* [1997] (interpolated to float position) and contemporaneous cloud reflectance values from the NASA Total Ozone Mapping Spectrometer averaged 98.8 and 100.2 W m^{-2},

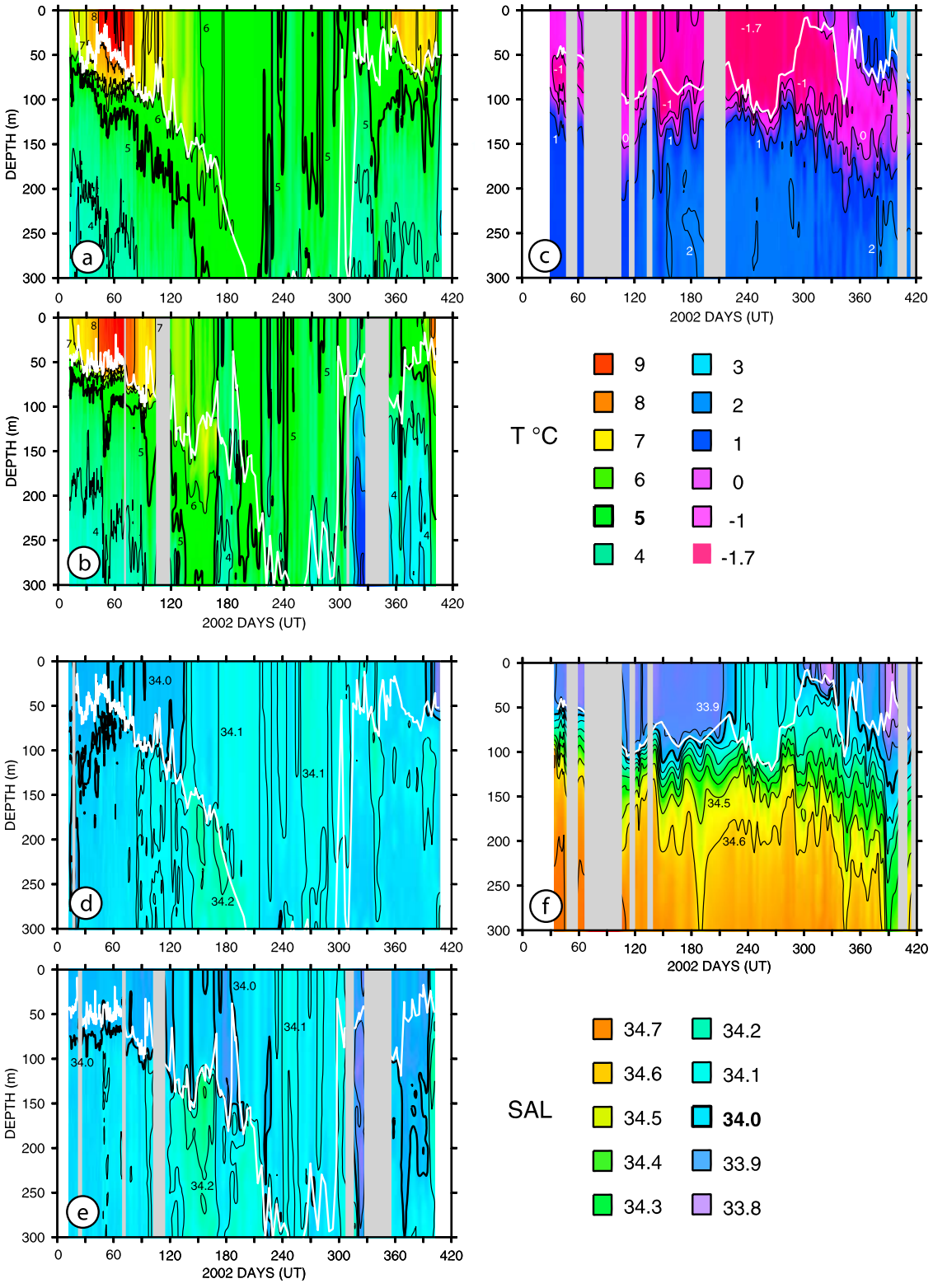

Figure 4. Time series observations of temperature for (a) CE 55A and (b) CE 55C deployed near 55°S, 172°W and for (c) CE 66A, deployed at 66°S, 172°W. Time series observations of salinity for (d) CE 55A, (e) CE 55C, and (f) CE 66A. The white line denotes the mixed layer depth based on a 0.05 potential density unit change ($MLD_{0.05}$). The vertical gray bars denote periods of incomplete data relay via ORBCOMM satellites. From day 240 to day 280, CE 66A salinity data indicate the formation of 0.5 m of sea ice. CE 55A passed through the Udintsev Fracture Zone (Figure 3) at nearly the same time as CE 66A in early January 2003, yet both saw the unique and very different water masses that they had been following.

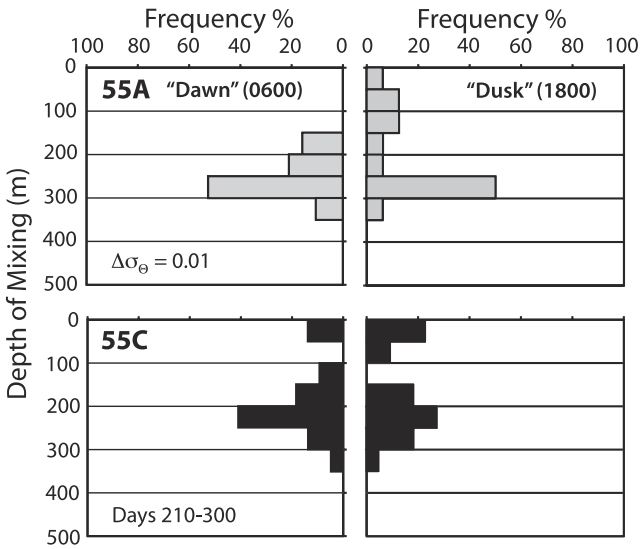

Figure 5. Frequency histogram of mixed layer depths ($MLD_{0.01}$) for (top) CE 55A and (bottom) CE 55C during the period of greatest mixed layer development (days 210–300). CE 55C's record indicated many more occurrences of transient shallow stratification of the upper 50 m.

respectively. The ~1.4% higher surface irradiance for CE 55A is consistent with its displacement ~1° equatorward of CE 55C during the time of deepest mixing. We could not estimate other heat budget components (especially latent heat) because of lack of atmospheric boundary layer conditions. Averages of T and S of near-surface waters were 5.00 and 4.90°C and 34.11 and 34.09‰ for CEs 55A and 55C, respectively. It is thus likely that minor differences in the complete air-sea heat budget (and possibly freshwater inputs) resulted in the differences in mixing depths observed.

3.1.3. Critical Depth

[23] Critical depth [*Sverdrup*, 1953] is the depth of mixing above which photosynthesis is sufficient to meet the energy requirements of the phytoplankton in the layer. We use the more realistic *Nelson and Smith* [1991] modification of the Sverdrup relationship, derived for the Southern Ocean, which considers the balance between photosynthesis and community respiration and sinking losses:

$$Z_{CRIT} = \sum \mathrm{PAR}_0/(3.78k_{PAR}). \quad (1)$$

[24] Daily averaged photosynthetically active radiation (PAR) arriving at the sea surface, PAR_0 (in E m^{-2} d^{-1}), is 47% of total daily solar irradiance [*Bishop et al.*, 1997]. The factor 3.78 in equation (1) combines separate factors for water surface albedo, the rapid attenuation of red light with

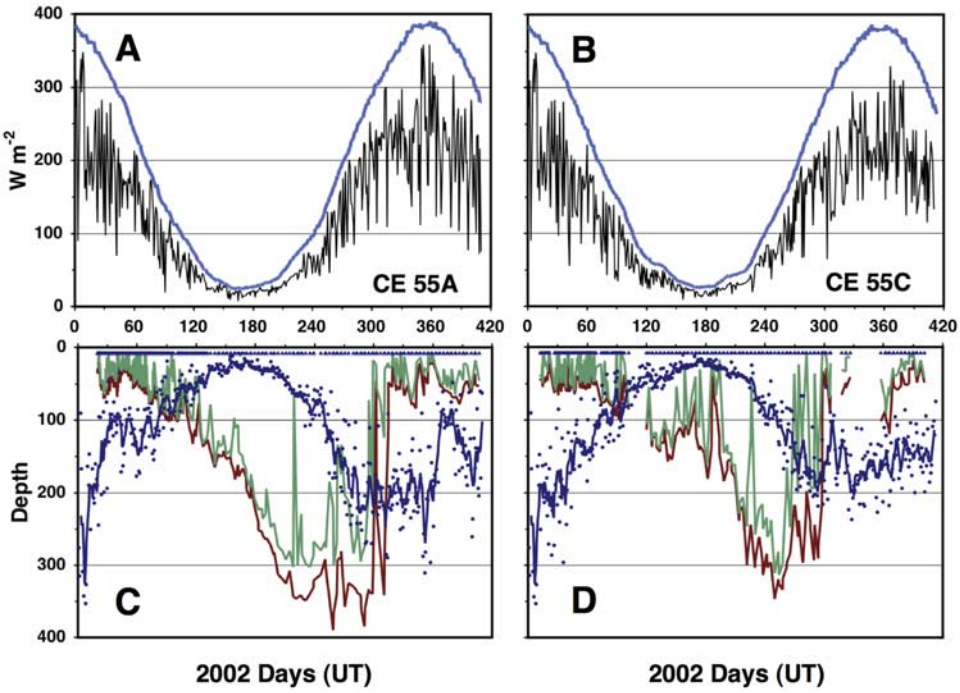

Figure 6. Surface shortwave solar irradiance estimated for positions of (a) CE 55A and (b) CE 55C. Blue, top line denotes irradiance under clear-sky conditions; black line is surface irradiance including the effects of clouds. (c) $MLD_{0.01}$ and (d) $MLD_{0.05}$. Green and red lines denote the time history of the mixed layer depths. Blue points show the critical depth calculated according to *Nelson and Smith* [1991]. The CE 55A time series showed almost no time when $MLD_{0.01}$ was shallower than critical depth from day 210 (May) to day 290 (late October). The CE 55C time series showed frequent occurrences when $MLD_{0.01}$ was shallower than critical depth. These times are when photosynthesis would exceed community respiration requirements in the mixed layer.

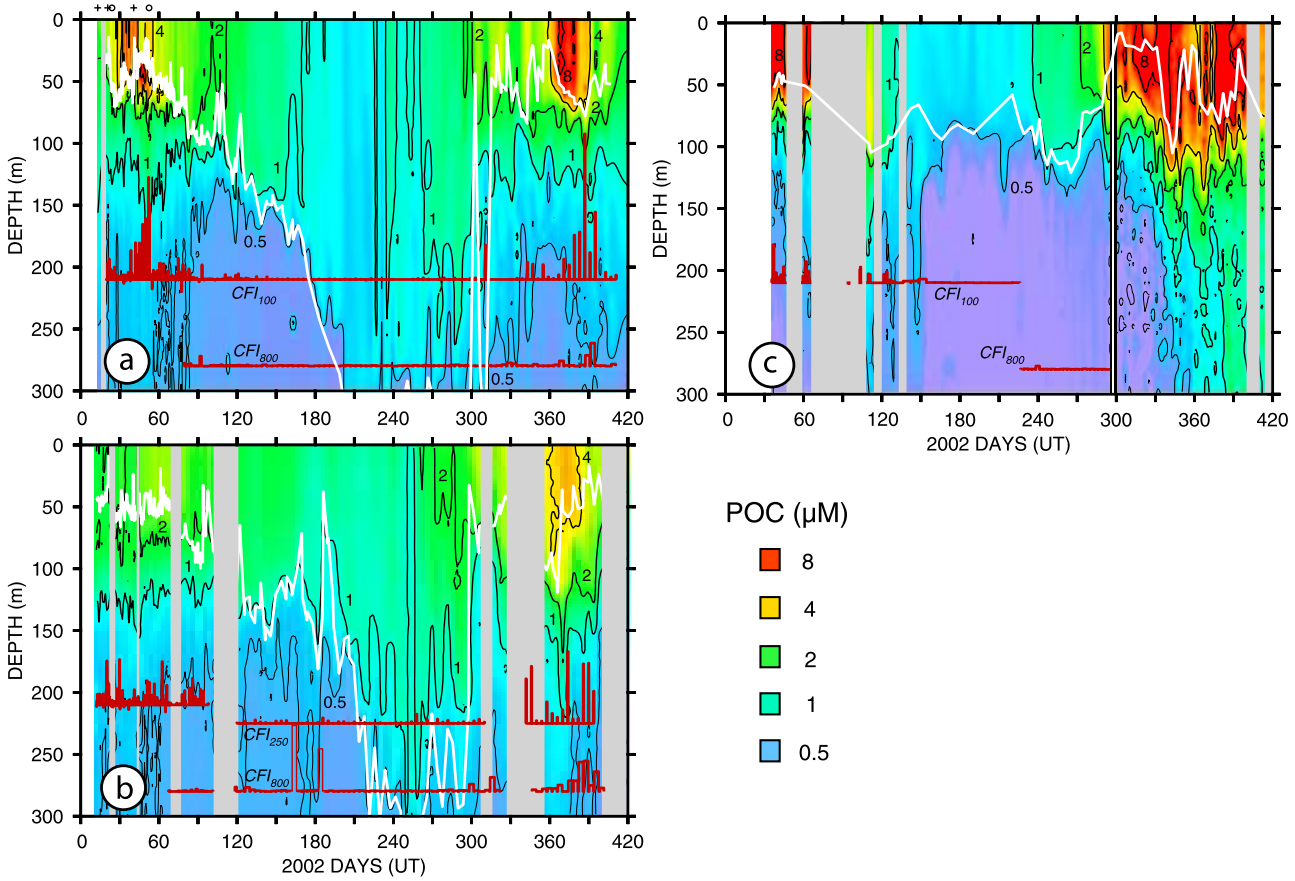

Figure 7. POC and carbon flux index time series for (a) CE 55A, (b) CE 55C, and (c) CE 66A. POC concentrations of 1, 2, 4, and 8 μM are contoured with heavy black lines; 0.5 μM is contoured by the thin black line. CFI is shown as red bars. Relative vertical placement denotes CFI readings at 100, 250, and 800 m. CE 55A data from day 10 to day 70 show the influence of iron added during the Southern Ocean Iron Experiment (SOFeX). The transmissometer on CE 66A was ice damaged on day 293; the POC time series beyond day 293 are estimated using data from the scattering sensor.

depth, and the net photocompensation irradiance (defined as that required to meet bacteria, phytoplankton, and zooplankton respiration and particle sinking loss terms) of 35 μE m^{-2} s^{-1}; the latter is roughly 10 times the respiration of the phytoplankton. Diffuse attenuation coefficient, k_{PAR}, is approximated from beam attenuation coefficient: $k_{PAR} = 0.027 + c_P 0.27$ (based on work by *Smith and Baker* [1981] and *Bishop et al.* [2002]).

[25] The derived critical depth time series is compared with MLD_{01} and MLD_{05} in Figure 6. MLD_{05} exceeded Z_{CRIT} throughout the winter mixing period (days 210–300) for both CE 55A and CE 55C time series. MLD_{01} showed rare occurrences shallower than Z_{CRIT} between days 210 and 270. Records for the two explorers diverged strongly from one another during the last month of deep mixing (days 270–300, October 2002), where MLD_{01} was shallower than Z_{CRIT} 15% and 60% of the time for CE 55A and CE 55C, respectively. Transient weak stratification had clearly resulted in conditions more favorable to a positive net community production-respiration balance in waters tracked by CE 55C during this time.

[26] How transient stratification and critical depth are linked to POC and CFI variability after establishment of permanent stratification is discussed in section 3.2.

3.2. POC and Export Variability North of the APF

[27] Figures 7a and 7b show the two 400 day long time series of POC concentration in the upper 300 m and CFI variability at 100, 250, and 800 m (CE 55C) and at 100 and 800 m (CE 55A), both deployed and operating north of the APF.

[28] The effects of SOFeX iron are seen in the distinctly different POC records for CE 55A (iron-amended) versus CE 55C (control) during the first 70 days of 2002. During this time, CE 55A showed that iron amendment had induced a fourfold increase and subsequent decline in POC (from 2 to 9 to 2 μM) and led to a fourfold enhancement of particle sedimentation at 100 m compared to POC and CFI records from CE 55C which served as a control [*Bishop et al.*, 2004]. After day 70 (11 March 2002), records from the two floats had become virtually indistinguishable in both POC and CFI and other hydrographic properties, suggesting loss of all effects of the SOFeX iron-enhanced water.

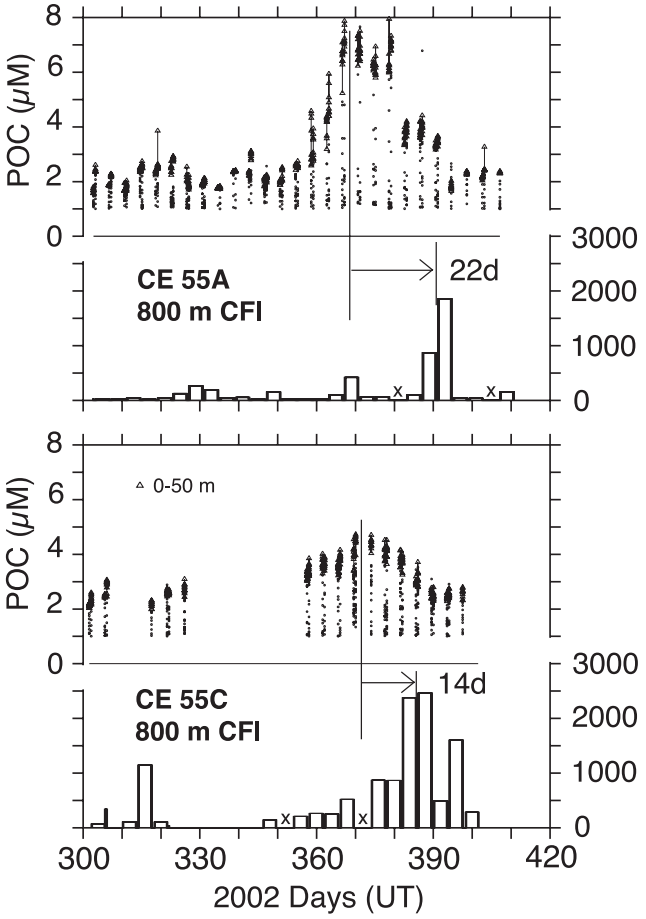

Figure 8. POC concentrations in waters shallower than 200 m (0–50 m data: triangles) for days 300 to 420 for (top) CE 55A and (bottom) CE 55C, compared with corresponding CFI data at 800 m. A reduced and more time lagged flux at 800 m occurred beneath the bloom observed by CE 55A. The 3 times stronger CFI peak at 800 m, 14 days after peak surface biomass observed by CE 55C, indicated a much more efficient carbon export to deep waters.

[29] Given the nearly identical conditions after day 70 at the end of summer, the question is, how would POC and CFI change with progression of season to winter and mixed layer deepening and upon restratification the following spring?

[30] With onset of deep winter mixing, both POC and CFI decrease as expected. During the period of deepest mixing (days 210 to 300), POC levels averaged over the daily mixed layer (MLD_{05}) had decreased to 0.7 (CE 55A) and 1 μM (CE 55C).

[31] Permanent shallow stratification was established near day 300, and peak near-surface biomass levels were observed 2 months later in early January 2003. POC concentration isolines in the waters of the relict deep mixed layer rapidly shifted to shallower depths, reflecting POC consumption and sedimentation losses [cf. *Bishop et al.*, 1986a]. POC and 100 m CFI in poststratification records of CE 55A were remarkable because both parameters almost exactly replicated the POC levels and CFI increases induced by iron during SOFeX 1 year earlier.

[32] In January 2003, CE 55C recorded a modest but significant twofold increase (relative to January 2002) of POC to 4 μM. CFI at 250 m was also stronger than observed 1 year earlier at shallower depths. CFI records at 800 m indicated a much greater flux than observed by CE 55A. The peaks in the 800 m CFI lagged the peaks of surface POC by approximately 22 and 14 days for CEs 55A (bloom) and 55C (nonbloom), respectively (Figure 8).

[33] The dynamic range of CFI at 800 m is comparable with organic carbon fluxes observed by deep moored sediment traps [*Honjo et al.*, 2000] from late 1996 through 1997 at Site MS-2 (982 m) 56°54′S, 170°W, the closest matchup to conditions sampled by CEs 55A and 55C. Flux variability averaged by traps over 17 to 51 days at MS-2 yielded a factor of 30 dynamic range. CFI values at 800 m, averaged over comparable periods during deep mixing and poststratification (days 375–415), were 53 and 1280 (CE 55C) and 41 and 400 (CE 55A) with dynamic ranges of 24 and 10, respectively. The agreement of results is reasonable given that these are the second and third yearlong records of sedimentation in these waters.

[34] Down the water column, peak CFI at 800 m lagged peak CFI at 100 m by approximately 7–10 days, suggesting particle settling rates of 70–100 m d^{-1}. This finding is also in reasonable agreement with estimates based on sediment traps deployed at depths of 982 and 4000 m at MS-2 [*Honjo et al.*, 2000]; however, unlike sediment traps, the CEs observed variations of POC in the water column and CFI over periods from 8 h to several days and relayed data to shore in near real time.

3.3. POC and Export Variability South of the APF

[35] CE 66A operated for 14 days below the iron-amended waters at 66°S. Unlike its northern cousin, it lost contact with the iron-amended surface layer rapidly because of strong shear in currents between the near-freezing winter water layer at 100 m in which it was parked and the warmer, less saline, iron-enriched waters of the upper 30 m (Figure 7c).

[36] Because of persistent winds and poor ORBCOMM service coverage, there was an almost continuous 60 day gap in observations from mid-February (day 45) through April 2002. Remarkably, data transmission was nearly 100% from mid-April to mid-October 2002 (days 115 to 290), when the float was operating in fully developed wintertime conditions in the presence of ice (Figure 9) and for much of that time in total darkness.

[37] Selected T, S, and POC profiles for different times over the history of the CE 66A record reveal strong temporal influences of mixing, production, settling, and respiration and of the formation and melting of sea ice (Figure 10).

[38] In mid-February 2002, POC in the upper 35 m was 10 μM and decreased rapidly with depth to below 0.2 μM by 250 m. On day 111 (21 April 2002), POC in the 100 m deep mixed layer was reduced to 4 μM. Meanwhile, POC levels at 150 m had increased by a factor of 2 from approximately 0.5 to 1.0 μM, and elevated POC concentrations were detected all the way down the water column to

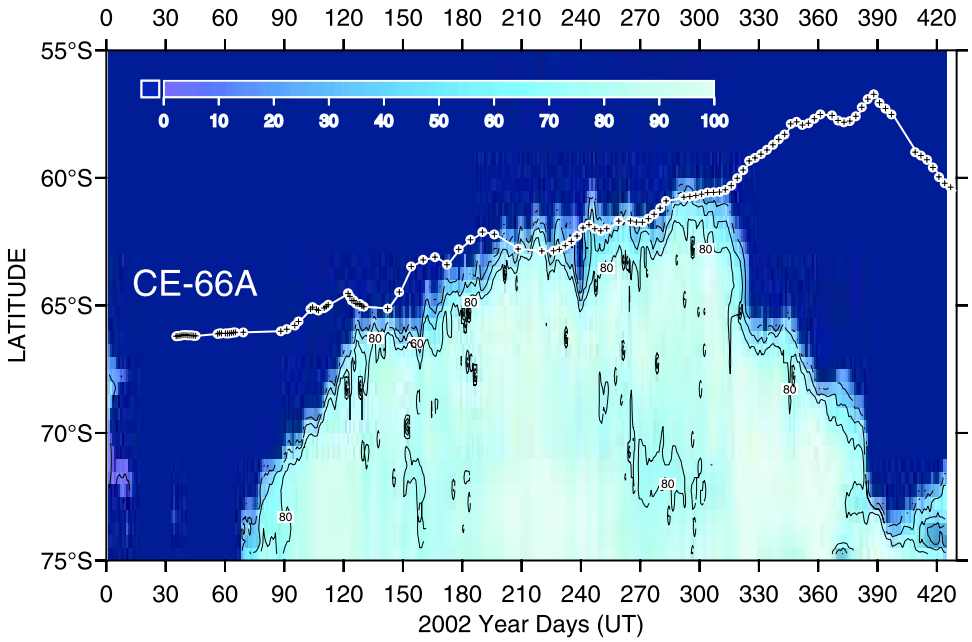

Figure 9. Time series of sea ice extent and percentage cover overlaid by the latitudinal position of CE 66A. Sea ice cover time series is derived at the longitude position of the explorer. CE 66A was in the ice edge zone for over 100 days. The color bar denotes ice percentages.

550 m. Ten days later, near-surface POC had decreased to ~1.3 μM, and most of the sub-mixed-layer POC anomaly had disappeared. The anomalous POC profile sampled on day 111 coincided with the onset of 24 h darkness, suggesting phytoplankton sinking had occurred in the weeks prior to the profile. The fact that 100 m CFI values (Figure 7c) were not particularly high and the fact that the elevated concentration anomaly did not propagate downward after day 111 suggest that most of the later POC loss was due to in situ consumption processes rather than sinking. On day 178 (28 June), in perpetual darkness, mixed layer POC was ~0.6 μM, and the entire deeper water column below 80 m was reduced to <0.2 μM.

[39] From days 180 to 230 (30 June to 18 August), surface temperature decreased by 0.7°C to the freezing point of seawater (−1.7°C), consistent with an average surface heat flux of −54 W m^{-2} d^{-1} (Figure 5c). Profiles from day 178 to day 250 showed a 0.2‰ salinity increase consistent with the formation of 0.5 m of sea ice (Figure 5f). Warming and ice melt began around day 280, and both thermal and salinity stratification became fully developed over the period from days 315 to 335 (11–30 November).

[40] With first light (day 215), surface POC levels began a slow rise to ~3.5 μM by day 292. On day 293 the transmissometer (or its electrical cable) was damaged while still operating in the presence of sea ice, ending usable POC and CFI data. However, the scattering sensor recorded the systematic variations of particle concentration for 200 more days. Its data, empirically calibrated with valid POC sensor data just prior to the ice event (Figure 7c), show strong resurgence of POC levels in response to ice melting induced stratification to ~9 μM. The time-dependent increase of subsurface POC concentrations (isolines at 120 m deepened to ~300 m between days 320 and 360) occurred when CE 66A was operating near 60°S.

4. Hypotheses to Explain Surface POC and Export Observations

[41] The biologically dynamic waters of the Southern Ocean are chronically underobserved yet are recognized as a highly important component of the global carbon cycle. The data we report here are the first year-round description of surface marine conditions, the evolution of surface biomass, and carbon sedimentation in the Southern Ocean.

[42] The fundamental observations to be explained are those at 55°S, where the two float "ensemble" time series showed contrasting conditions of deep particle sedimentation. Contrary to expectation, sedimentation at 800 m was 3 times lower in absolute terms beneath the blooming waters, as observed by CE 55A, compared to that observed by CE 55C, thus indicating much less efficient particle export when surface carbon biomass is enhanced. If we normalize to the strength of the surface POC maximum, the difference increases sixfold. The longer time lag between biomass maximum and sedimentation also suggests greater remineralization efficiency at a given depth beneath the bloom. We explore linkages and four hypotheses that would explain our observations.

[43] 1. A first hypothesis (H1) is that the CE 55A versus 55C records could be biased by the fact that there was an along-track current shear of ~8 km d^{-1} between 100 and 800 m (section 3.1) during the bloom and sedimentation events. In other words, was our result an artifact of spatial differences in overhead biomass versus subsurface flux? To test this hypothesis, we analyzed remotely sensed

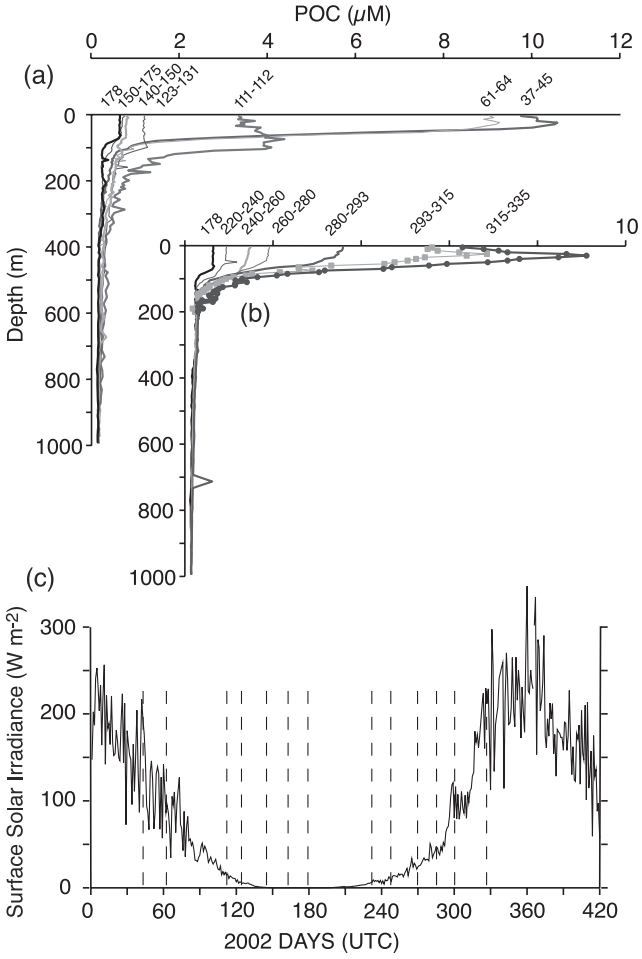

Figure 10. (a) Selected POC profiles from CE 66A from days 30 to 180. The effects of particle settling which enriched the water column to 600 m are seen on day 111 (21 April 2002). This enrichment was rapidly lost. Lowest POC levels were seen on day 178 (28 June 2002). (b) Selected POC profiles for days 180 to 320. Profiles with symbols are interpolated from scattering sensor data. (c) Solar irradiance time series for location of CE 66A. Vertical dashed lines correspond to times of POC profiles.

chlorophyll data at 9 km resolution (and daily frequency) for the period July 2002 through March 2003 from the merged observations by the NASA Moderate Resolution Imaging Spectroradiometer (MODIS) on the Aqua satellite and by the Sea-viewing Wide Field-of-view Sensor (SeaWiFS) satellite. Data were analyzed at various spatial domains of 81, approximately 600, and 4200 km^2 (1, 3×3, and 9×7 pixels). We set the positions for both CE 55A and CE 55C to those they had occupied 3.5 days prior to and 3.5 days after the time of actual observations and retrieved remotely sensed data for those positions. We chose the net 7 day difference because this is the approximate transit time for particles settling from 100 to 800 m. The resulting satellite data (auxiliary material Figure S1), although suffering temporal gaps due to storms, show surface chlorophyll temporal trends similar to the CE surface POC data with zero time lag.[1] The duration of bloom in waters in which CE 55A was operating was much longer than that for CE 55C. Furthermore, expansion of spatial domain revealed even higher chlorophyll around CE 55A than around CE 55C. Thus, the finding of lower 800 m export below areas of higher biomass is corroborated by this analysis. H1 is considered unlikely.

[44] 2. A second hypothesis (H2) is that the relative lack of CFI signal at 800 m for CE 55A versus CE 55C could be due to nondetection of "rare large particles" carrying most of the flux in one case but not the other. In other words, was the systematic use of the CFI signal invalid? While large particles may be relatively rare in the water column compared to smaller particles (abundancewise), these particles contribute to sedimentation (flux), which the CFI observations are intended to follow (see *Bishop et al.* [1978, 1986b] for discussion of in situ large particle concentration versus vertical flux). Recent results of *Ebersbach and Trull* [2008] in biologically dynamic waters near Kerguelen in the Southern Ocean demonstrate that volume flux is dominated by particulates smaller than 1 mm in size. Furthermore, in subeuphotic layer waters below blooms, large, millimeter-sized aggregates and fecal pellets (known to be sinking) are easily observed in high-concentration abundances but rapidly disappear with depth [*Lam and Bishop*, 2007]. A possible added contributor to the misconception of "rare large particles" is that some commonly used in situ particle-sampling systems appear to lose large particle samples [*Bishop and Wood*, 2008]. H2 is considered unlikely.

[45] 3. A third hypothesis (H3) is that the difference in POC and CFI time series between the two CEs is due to differences of macronutrient or micronutrient elements entrained into the surface layer after the deep winter mixing. In other words, does natural nutrient and iron fertilization explain the observations? The waters which CEs 55A and 55C were following are never nitrate- or phosphate-limited. For example, nitrate levels observed by SOFeX [*Coale et al.*, 2004] in iron-amended waters at 55°S had not decreased below 18 μM. Silicate was considered limiting, and SOFeX iron had reduced concentrations from 4 to $\sim$1 μM. Observations in similar waters (58°S and 96°W; April 1995) showed 20 μM, 1.5 μM, 3 μM, and $\sim$0.3 nM nitrate, phosphate, silicate and iron, respectively, in a mixed layer to 150 m and 28 μM, 2 μM, 20 μM, and 0.3 nM, respectively, at 400 m [*de Baar et al.*, 1999]. If we used these data as proxy, then wintertime mixing (CE 55C at 375 m versus CE 55A at 435 m) would have had almost no effect on iron, a small effect on nitrate and phosphate ($\sim$3%), and the greatest effect on silicate ($\sim$20%). Post-winter mixing concentrations of nutrients in surface waters would be 22.1 and 22.8 μM nitrate and 7.5 and 9.0 μM silicate for CEs 55C and 55A, respectively, and $\sim$0.3 nM for iron for both. We cannot 100% rule out H3 for iron effects because of extremely scant metal data availability for the Southern Ocean; however, if iron triggered the bloom, then sedimentation at depth is suppressed by iron.

[1] Auxiliary materials are available in the HTML. doi:10.1029/2008GB003206.

[46] 4. The fourth hypothesis (H4) is that the two different outcomes at 55°S critically depend on the observation of differences in the frequency of transient stratification events during the period of greatest wintertime mixing. In other words, waters tracked by CE 55C experienced greater light, leading to an enhancement of photosynthesis to the benefit of overwintering zooplankton populations. As the critical depth comparison shows (Figure 7), phytoplankton tracked by CE 55C received more than sufficient solar energy to allow for net growth, particularly during the 30 day period prior to permanent stratification. The POC levels reflected this enhanced growth.

[47] The question is, how was enhanced productivity passed on to the zooplankton community resident in the deep mixed layer? There is abundant literature on Antarctic zooplankton, but to the best of our knowledge, there have been no studies of zooplankton growth during periods of deep mixing in the Southern Ocean. We do, however, have observations of particulate carbon, chlorophyll, and zooplankton growth behavior and deep mixing during late winter and early spring in the North Atlantic. Enhanced stocks of chlorophyll and zooplankton biomass were observed in a 400 m deep (but frequently transiently stratified) mixed layer during an intensive multiship, multiseason campaign to study Gulf Stream warm core ring (WCR) 82B in the NW Atlantic [*Bishop et al.*, 1986a, 1992]. In the case of WCR 82B, zooplankton biomass in the deep layer was observed to increase by over 250% over a 40 day period prior to permanent stratification. Just prior to stratification, integrated stocks of chlorophyll in the deep mixed layer equaled that of nearby stratified waters undergoing a bloom. The increase of zooplankton biomass in this deeply mixed and chlorophyll-rich regime suggests that they were well nourished. We hypothesize that zooplankton in the deep layer observed by CE 55C derived a relative benefit.

[48] In contrast, CE 55A records showed that the mixed layer depth exceeded critical depth until day 300 (late September 2002) with an almost instantaneous transition to a state of permanent shallow stratification. The zooplankton community within this deep layer is thus hypothesized to be in a state of relative starvation, consistent with the Nelson-Smith critical depth formulation. With permanent stratification, the less developed zooplankton community could not keep pace with the burst in plant growth in surface waters, thus leading to a classic bloom condition.

[49] A hypothesized more nourished and relatively enhanced overwintering zooplankton community of CE 55C's water column was thus better able to synchronize with the faster growing phytoplankton in surface waters and largely quench the bloom before it developed.

[50] The further consequence of a relatively starved zooplankton community in CE 55A's water column was a more efficient particle harvesting (and shorter remineralization length scale) and thus a strongly reduced CFI at 800 m. The consequence of the hypothesized better fed community in CE 55C's water column was less efficient assimilation and thus a much greater flux at 800 m. The CE results reinforce *Lam and Bishop*'s [2007] hypothesis (based on limited ship observations) that high surface carbon (and chlorophyll) phytoplankton biomass counterindicates deep carbon sedimentation.

[51] *Siegel et al.* [2002] have also investigated critical depth theory and described anomalies of the timing of the initiation of the North Atlantic spring bloom seen in SeaWiFS data versus the expected bloom initiation computed using critical depth, derived using monthly mean mixed layer depths (MLD_{125}). They assumed that the production-loss balance must be in steady state prior to initiation of the bloom and that bloom trajectories in time are determined by the zooplankton growth response at the time of transition of MLD_{125} to shallower than Z_{CRIT}; a fast growing community could thus quench a bloom. Our observations point to the importance of transient wintertime stratification in setting the very conditions that would permit prestratification zooplankton growth and thus the development of a bloom-quenching grazing community.

[52] The strongest hypothesis is H4. H3 is unlikely but possible, and both H1 and H2 are considered very unlikely.

5. Conclusion

[53] Natural processes are inherently nonlinear and sensitive to small perturbations. Our results described in section 3 furthermore demonstrate the exquisite sensitivity. The two 55°S CEs were calibrated with one another and were deployed in initially identical hydrographic conditions. Subtle differences in ocean physical forcing along their trajectories induced slight perturbations, which over the winter led to very distinct biological responses after seasonal stratification of the water column. We had, in other words, performed a very modest ensemble experiment.

[54] As the CEs were relatively low cost (each costing the equivalent of one day of ship time), a larger-scale ensemble experiment is both feasible and desired to answer questions that may linger about the generalizations we have made. H4 would be supported by a robust coherence of POC and CFI behavior and stratification history, for example. Analysis of the carbon outcomes of a larger ensemble would yield meaningful statistics of organic carbon inventories and the relationship among surface forcing, surface biomass (a remotely sensed ocean property), hydrographic conditions, and carbon export. These statistics could be compared to results from models that do not capture the high-frequency or subgrid variability in the biological pump. Such observation ensembles will build confidence in new parameterizations of biological pump processes and lead to a quantum gain in understanding and predictability of processes important to ocean carbon. It is now possible to address the larger question of whether or not the substantial biologically mediated carbon flows to the deep sea are in steady state.

[55] **Acknowledgments.** This research has been supported by the U.S. Department of Energy, Office of Science, Biological and Environmental Research Program, and by the National Oceanographic Partnership Program administered by ONR. Russ Davis and Jeffrey Sherman (Scripps Institution of Oceanography, Instrument Development Group) and WETLabs, Inc., played critical roles in creating the Carbon Explorer. We acknowledge contributions of the three anonymous reviewers of this paper. We also thank Kenneth Coale (lead PI of Southern Ocean Iron Experiment) and Ken Johnson, chief scientist, and crew aboard R/V *Revelle* during SOFeX.

References

Abbott, M. R., J. G. Richman, J. S. Nahorniak, and B. S. Barksdale (2001), Meanders in the Antarctic Polar Frontal Zone and their impact on phytoplankton, *Deep Sea Res., Part II*, *48*, 3891–3912, doi:10.1016/S0967-0645(01)00073-X.

Antoine, D., J.-M. Andre, and A. Morel (1996), Oceanic primary production: 2. Estimation at global scale from satellite (coastal zone color scanner) chlorophyll, *Global Biogeochem. Cycles*, *10*, 57–69, doi:10.1029/95GB02832.

Argo Science Team (1999), On the design and implementation of Argo: A global array of profiling floats, *Rep. 21*, 35 pp., Int. CLIVAR Proj. Off., Southampton, U. K.

Armstrong, R. A., C. Lee, J. I. Hedges, S. Honjo, and S. G. Wakeham (2001), A new, mechanistic model for organic carbon fluxes in the ocean based on the quantitative association of POC with ballast minerals, *Deep Sea Res., Part II*, *49*, 219–236, doi:10.1016/S0967-0645(01)00101-1.

Bishop, J. K. B., and T. J. Wood (2008), Particulate matter chemistry and dynamics in the twilight zone at VERTIGO ALOHA and K2 Sites, *Deep Sea Res., Part I*, *55*, 1684–1706, doi:10.1016/j.dsr.2008.07.012.

Bishop, J. K. B., D. R. Ketten, and J. M. Edmond (1978), The chemistry, biology and vertical flux of particulate matter from the upper 400 m of the Cape Basin in the S.E. Atlantic Ocean, *Deep Sea Res.*, *25*, 1121–1161, doi:10.1016/0146-6291(78)90010-3.

Bishop, J. K. B., M. H. Conte, P. H. Wiebe, M. R. Roman, and C. Langdon (1986a), Particulate matter production and consumption in deep mixed layers: Observations in a warm core ring, *Deep Sea Res., Part A*, *33*, 1813–1841, doi:10.1016/0198-0149(86)90081-6.

Bishop, J. K. B., J. C. Stepien, and P. H. Wiebe (1986b), Particulate matter distributions, chemistry and flux in the Panama Basin: Response to environmental forcing, *Prog. Oceanogr.*, *17*, 1–59, doi:10.1016/0079-6611(86)90024-8.

Bishop, J. K. B., R. C. Smith, and K. S. Baker (1992), Springtime distributions and variability of biogenic particulate matter in Gulf Stream warm-core ring 82B and surrounding N.W. Atlantic waters, *Deep Sea Res.*, *39*, suppl. 1., S295–S325.

Bishop, J. K. B., W. B. Rossow, and E. G. Dutton (1997), Surface solar irradiance from the International Satellite Cloud Climatology Project 1983–1991, *J. Geophys. Res.*, *102*, 6883–6910.

Bishop, J. K. B., R. E. Davis, and J. T. Sherman (2002), Robotic observations of dust storm enhancement of carbon biomass in the North Pacific, *Science*, *298*, 817–821, doi:10.1126/science.1074961.

Bishop, J. K. B., T. J. Wood, R. E. Davis, and J. T. Sherman (2004), Robotic observations of enhanced carbon biomass and export at 55°S during SOFeX, *Science*, *304*, 417–420, doi:10.1126/science.1087717.

Bower, A. S., and W. J. von Appen (2008), Interannual variability in the pathways of the North Atlantic current over the Mid-Atlantic Ridge and the impact of topography, *J. Phys. Oceanogr.*, *38*(1), 104–120, doi:10.1175/2007JPO3686.1.

Bower, A. S., B. Le Cann, T. Rossby, W. Zenk, J. Gould, K. Speer, P. L. Richardson, M. D. Prater, and H. M. Zhang (2002), Directly measured mid-depth circulation in the northeastern North Atlantic Ocean, *Nature*, *419*, 603–607, doi:10.1038/nature01078.

Buesseler, K. O., et al. (2007), Revisiting carbon flux through the ocean's twilight zone, *Science*, *316*, 567–570, doi:10.1126/science.1137959.

Coale, K. H., et al. (2004), Southern Ocean Iron enrichment experiment: Carbon cycling in high- and low-Si waters, *Science*, *304*, 408–414, doi:10.1126/science.1089778.

Davis, R. E. (2005), Intermediate-depth circulation of the Indian and South Pacific oceans measured by autonomous floats, *J. Phys. Oceanogr.*, *35*(5), 683–707, doi:10.1175/JPO2702.1.

de Baar, H. J. W., J. T. M. de Jong, R. F. Nolting, K. R. Timmermans, M. A. van Leeuwe, U. Bathmann, M. R. van der Loeff, and J. Sildam (1999), Low dissolved Fe and the absence of diatom blooms in remote Pacific waters of the Southern Ocean, *Mar. Chem.*, *66*, 1–34, doi:10.1016/S0304-4203(99)00022-5.

Ebersbach, F., and T. W. Trull (2008), Sinking particle properties from polyacrylamide gels during the Kerguelen Ocean and Plateau compared Study (KEOPS): Zooplankton control of carbon export in an area of persistent natural iron inputs in the Southern Ocean, *Limnol. Oceanogr.*, *53*, 212–224.

Falkowski, P. G., R. Barber, and V. Smetacek (1998), Biogeochemical controls and feedbacks on ocean primary production, *Science*, *281*, 200–206, doi:10.1126/science.281.5374.200.

Feely, R., C. L. Sabine, K. Lee, W. Berelson, J. Kleypas, V. J. Fabry, and F. J. Millero (2004), Impact of anthropogenic CO_2 on the $CaCO_3$ system in the oceans, *Science*, *305*, 362–366, doi:10.1126/science.1097329.

Field, C. B., M. J. Behrenfeld, J. T. Randerson, and P. G. Falkowski (1998), Primary production of the biosphere: Integrating terrestrial and oceanic components, *Science*, *281*, 237–240, doi:10.1126/science.281.5374.237.

Honjo, S., R. Francois, S. Manganini, J. Dymond, and R. Collier (2000), Particle fluxes to the interior of the Southern Ocean in the western Pacific sector along 170°W, *Deep Sea Res., Part II*, *47*, 3521–3548, doi:10.1016/S0967-0645(00)00077-1.

Lam, P. J., and J. K. B. Bishop (2007), High biomass low export regimes in the Southern Ocean, *Deep Sea Res., Part II*, *54*, 601–638, doi:10.1016/j.dsr2.2007.01.013.

Martin, J. H., G. A. Knauer, D. M. Karl, and W. W. Broenkow (1987), VERTEX: Carbon cycling in the northeast Pacific, *Deep Sea Res., Part A*, *34*(2), 267–285, doi:10.1016/0198-0149(87)90086-0.

Morrison, J. M., S. Gaurin, L. A. Codispotti, T. Takahashi, F. J. Millero, W. D. Gardner, and M. J. Richarson (2001), Seasonal evolution of hydrographic properties in the Antarctic Circumpolar Current at 170°W during 1997–1998, *Deep Sea Res., Part II*, *48*, 3943–3972, doi:10.1016/S0967-0645(01)00075-3.

Nelson, D. M., and W. O. Smith Jr. (1991), Sverdrup revisited: Critical depths, maximum chlorophyll levels, and the control of Southern Ocean productivity by the irradiance-mixing regime, *Limnol. Oceanogr.*, *36*, 1650–1661.

Orr, J. C., et al. (2005), Anthropogenic ocean acidification over the twenty-first century and its impact on calcifying organisms, *Nature*, *437*, 681–686, doi:10.1038/nature04095.

Sabine, C. L., et al. (2004), The ocean sink for anthropogenic CO_2 in the ocean, *Science*, *305*, 367–370, doi:10.1126/science.1097403.

Siegel, D. A., S. C. Doney, and J. A. Yoder (2002), The North Atlantic spring phytoplankton bloom and Sverdrup's critical depth hypothesis, *Science*, *296*, 730–733, doi:10.1126/science.1069174.

Smith, R. C., and K. S. Baker (1981), Optical properties of the clearest natural waters (200–800 nm), *Appl. Opt.*, *20*, 177–184, doi:10.1364/AO.20.000177.

Sverdrup, H. U. (1953), On conditions for the vernal blooming of phytoplankton, *J. Cons. Cons. Int. Explor. Mer*, *18*, 287–295.

Volk, T., and M. I. Hoffert (1985), Ocean carbon pumps: Analysis of relative strengths and efficiencies in ocean-driven atmospheric CO_2 changes, in *The Carbon Cycle and Atmospheric CO_2: Natural Variations Archean to Present*, *Geophys. Monogr. Ser*, vol. 32, edited by E. T. Sunquist and W. S. Broeker, pp. 99–110, AGU, Washington, D. C.

J. K. B. Bishop, Department of Earth and Planetary Science, University of California, 307 McCone Hall, Berkeley, CA 94720, USA. (jkbishop@berkeley.edu)

T. J. Wood, Earth Sciences Division, Lawrence Berkeley National Laboratory, 1 Cyclotron Road, MS 90-1116, Berkeley, CA 94720, USA. (tjwood@lbl.gov)